Imperial College London
Institute for Molecular Science and Engineering

Research Article

# Microfluidic-based wearable monitoring system for sweat sensing

by

Yiluo Li

CID: 02168459

Email: yiluo.li21@imperial.ac.uk

Supervisors:

Prof. Pantelis Georgiou

Prof. Alison Holmes

External Partner:

Imperial College Healthcare NHS Trust

September 2022

# Microfluidic-based wearable monitoring system for sweat sensing

Yiluo Li,[a] Anirban Sinhamahapatra,[b] Daryl Ma,[b] Pantelis Georgiou*[b] and Alison Holmes* [c]

Wearable devices based on microfluidic technology make it possible to do parallel and non-invasive monitoring of body condition with a small amount of sample. Many soft skin-interfaced wearable devices are reported to measure basic physiological data such as pH value, secretory fluidic pressures, sweat loss and so on. This paper introduces two devices which have the potential to be used in sweat sensing: (1) A PDMS sweat collection patch with microfluidic channels and multiple chambers which can be embedded with paper-based assays for colorimetric analysis. (2) A 3D-printed flip-cover sensor carrier with microfluidic sweat collection. Besides, the research also includes: (1) The precision and thickness fabrication control of photolithography are discussed. (1) Capillary bursting valves (CBVs) which can drive sweat into chambers sequentially are introduced in microfluidic device to allow a continuous analysis and the relation between bursting pressure and width of valve is defined. (3) To achieve spontaneous flow of sweat in microfluidic channels, surface modification by air plasma is studied and potential modification method based on thiol-ene click reaction is proposed. The results provide a basis for further improvements of device design and fabrication.

*a. Institute for Molecular Science and Engineering, Imperial College London.*
*b. Centre for Bio-Inspired Technology, Department of Electrical and Electronic Engineering, Imperial College London.*
*c. Department of Infectious Disease, Imperial College London.*
*d. External Partner: Imperial College Healthcare NHS Trust.*

# Introduction

In twenty-first century, the concept of health has gradually changed from 'diagnosis and treatment from doctor' to 'disease-free prevention and intervention therapy'. (1) In this case, real-time monitoring of body status is essential. Emerging capabilities in materials, electronics, data interaction, and ergonomics enable many companies to develop wearable devices with health innovations such as Google Glass, Apple iWatch, and Nike Adapt. (2,3) The existing commercial devices are capable of monitoring blood oxygen level and heart rate.(4) However, more complicated physiological parameters are demanded for disease diagnosis. The concentration of biomarkers contained in biofluids are regarded as indicators of diseases. Sweat, one of the most representative biofluids, offers sufficient information about biomarkers including electrolytes, nitrogenous compounds, and xenobiotics. (5) Compared with blood, sweat can be collected via non-invasive method with skin-interfaced microfluidic patch contacted with wide distribution of sweat glands. The enrich biomarkers contained in sweat provide meaningful and objective information about health status. Many research works have been done to demonstrate the pH value, secretory fluidic pressure, sweat loss, and concentrations of biomarkers such as creatine by 'epidermal' platform with the help of electronics or unique designed structure. (6,7) The concentration of these detected objects can illustrate basic health problems, for example, preliminary diagnosed with hyperhidrosis by analysing sweat production rate, diabetes by analysing the concentration of glucose as well as stress or fatigue by concentration of cortisol.(7,8)

Microfluidics, as an emerging technology, has been applied to many fields especially for sensing processes with advantages of miniaturization and parallelism. (9)

Microfluidics can manipulate fluids in micrometre scale by combing effect of valves, pumps along with the design of microchannels. (9) Common sampling method for analyte sensing in biological fluid has a huge demand for sample volume resulting in incapability of portability and dynamicity. (10) By introducing the wearable microfluidic platform, the above shortcomings of traditional method will be overcome due to features as high-throughput and miniaturization of microfluidics. (11) There are many methods have been used to develop microfluidics, for example as 3D printing, laser cutting and photolithography. (7,12,13)

Generally, the minimum feature size for 3D printing should be more than 200 microns. (14) In contrast, sub-micron printing can be achieved by photolithography which is more precise. (15)

For wearable devices, there are many requirements for materials such as flexibility. PDMS is the most used material for wearable microfluidic devices with the advantages of its biocompatibility, mechanical stability, gas permeability, and satisfactory optical transparency. (16) Besides, the smallest channel dimension of PDMS can be less than 100nm which is far superior to other materials for example as silicones and hydrogels. (16)

Although PDMS is an ideal material for wearable devices, it is difficult for sweat to flow spontaneously in channels due to its nature hydrophobicity when collecting sweat from skin. However, it is known that liquid flows into channels driven by intermolecular forces due to capillary motion. Thus, three solutions (surface modification, introducing capillary bursting valves or chemical pump) by means of capillary action are studied. (17–19) Surface with high surface energy is more easily for wetting and capillary spreading. (20) By introducing hydrophilic groups, the surface of channels in wearable device can exhibit an excellent hydrophilic and wetting for spontaneous sweat collection. (18)

The following introduces two wearable devices which are potential for sweat sensing. The first device is a soft PDMS patch with four reservoirs which can be embedded with assays for colorimetric analysis. Capillary bursting valves designed in microchannels can drive sweat into chamber sequentially. The device is fabricated by photolithography and preliminary surface modification is completed by plasma treatment. The second device consists of a 3D-printed chip carrier and a skin-mounted patch with flower-shaped micro-channels for sweat collection.

# Methodology

**3D printing of sensor carrier**

The device was designed by AutoCAD software (onshape). A MultiJet Printer (ProJet MJP 2500, 3D Systems, US) and Material M2S-HT90 were used to print the sensor carrier.

The platform with printed stuff was placed on hot plate to melt the wax between printed stuff and platform. The remaining wax was melted by hot steam and oil (Easy Clean, 3D Systems, US). The oil was dissolved in water with dish soap.

**Fabrication of microfluidic layer mould**

The desired pattern was designed by AutoCAD and the file was converted into machine format (**Figure 1.** step 1). A silicon wafer was bathed in acetone (Lp Chemicals, UK) and IPA (Isopropanol, 99.5%, Thermo Scientific™, UK) for 30s sequentially to remove the dirt, dried with air gun and placed on a hotplate at 150 ℃ for 15 min to remove remaining moisture. After cooling down, SU8 photoresist (SU8-2150, KAYAKU, US) was poured slowly on centre of wafer and avoid the formation of bubbles. A thin and flat photoresist layer was formed on the wafer via spin coater (Spin Coater WS-650MZ Modular, Laurell, US). After a pre-exposure bake on hotplate, the wafer with photoresist was exposed by UV printer (Smart Print UV, Microlight3D, France) (Figure 1. step 2). After a post-exposure bake (Hot plate, EMS1000-1, Electronic Micro Systems, UK), the unexposed photoresist was dissolved by developer and exposed part cured and become rigid (**Figure 1.** step 3).

**PDMS mould thickness measurements**

Three SU8 photoresist with different viscosities were used to develop PDMS mould. The thickness of PDMS mould was measured using an optical profilometer (The Profilm3D®, Filmetrics). The average thickness was based on three independent positions.

**Fabrication of microfluidic layer**

The patterned silicon wafer was bathed in IPA for 30s and dried with air gun. The base (SYLGAED™ 184 Silicone Elastomer Base, Dow, US) and curing agent (SYLGAED™ 184 Silicone Elastomer Curing Agent, Dow, US) (Tattersall 2002)(10:1) were mixed with glass rod until the mixture change from transparent into white and contains uniform bubbles. A vacuum desiccator (F42010-0000, Bel-Art, US) was used to pump out air periodically in mixture until no bubbles formed. The prepolymer was poured slowly on the patterned wafer and spread uniformly automatically (**Figure 1.** step 4). Then, the wafer was put into an oven (Fistreem Vacuum Oven, VAC1600, Gallenkamp, UK) at 65 ℃ for 12h. After cooling down, the surface of PDMS was non-sticky. Patterned part and a unppaterend part with equal size as capping layer were peeled off carefully by scalpel (**Figure 1.** step 5). The hole at inlet was formed by a circular punch with a diameter of 1.5 mm (BIOPSY punches, BPP-15F, KAI, Japan) (**Figure 1.** step 6). The capping layer was bonded to the microfluidic layer by exposure to air plasma (Harrick Oxygen Plasma Cleaner, PDC-32G-2, Harrick Plasma, US) (**Figure 1.** step 7).

**Plasma treatment for surface modification**

The PDMS samples were subjected to plasma treatment for 1min, 5min, 10min and 30 min, respectively. Contact angles of PDMS surface were measured after treatment immediately. The treated sample and pristine sample were placed at ambient temperature for 5 mins, 20mins, 30min 60min, 120min and 24hours. The changes of contact angles were recorded.

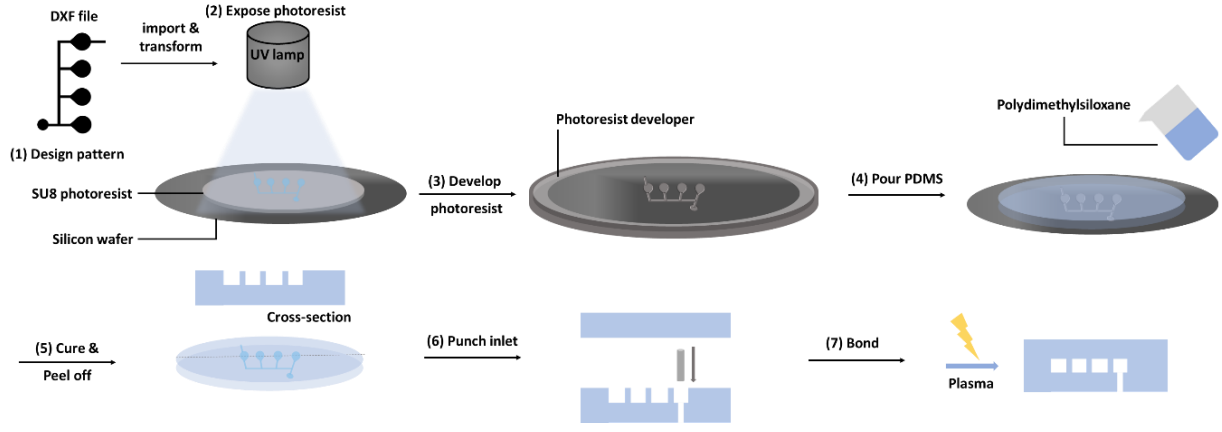


**Figure 1.** The schematic diagram of photolithography and microfluidic layer fabrication process.

## Results and discussion

### Epidermal patch for colorimetric analysis

The epidermal patch for colorimetric analysis as **Figure 2. a** is composed of three layers: (1) a PDMS capping layer, (2) a microfluidic layer with channels, four chambers and an outlet and (3) a layer with an inlet mounted on skin. The device is ~ 1.45 mm thick and is designed in a square with a side length of ~ 35mm. A PDMS capping layer with a thickness of ~0.65 mm seals the whole device. The microfluidic layer with a thickness of ~0.80 mm includes microchannels (~400 μm in width) and chambers (~3 mm in radius). Capillary bursting valves (CBVs) shown as **Figure 2. c** are designed to block the sweat flow until the chambers before them are fully filled as **Figure 2. e**. Thus, four chambers are filled with sweat in sequence (labelled $T_1$, $T_2$, $T_3$, $T_4$) shown as **Figure 2.b**. The sequential collection allows a continuous and staged sensing of sweat. Paper-based assays such as pH or enzyme assays can be embedded into chambers for colorimetric analysis as **Figure 2. a**. The patch with a small thickness and mechanical stability avoids separation from skin when bending as **Figure 2.d.**

### Photolithography for microfluidic layers

Three widths (400 μm, 600 μm and 800 μm**)** of channels as **Figure 3. a** are designed and fabricated to measure the accuracy of lithography process. The images of channels fabricated on PDMS mould and PDMS were captured by optical microscope (**Figure 3. b**) and the widths of channels were manually measured by Image J. In **Figure 3. c**, the widths of channels fabricated are oscillates around the designed value. The relative error of widths of channels on PDMS mould is 0.8% while the relative error for that of PDMS mould is 1%, which is slightly larger than the former. The cause of such error might be reduced resolution due to prolonged use of UV light or manual measurement by Image J. The widths of channels for wearable device are between 400 μm to 1000 μm, thus such small errors would not have a major impact on sweat collection.

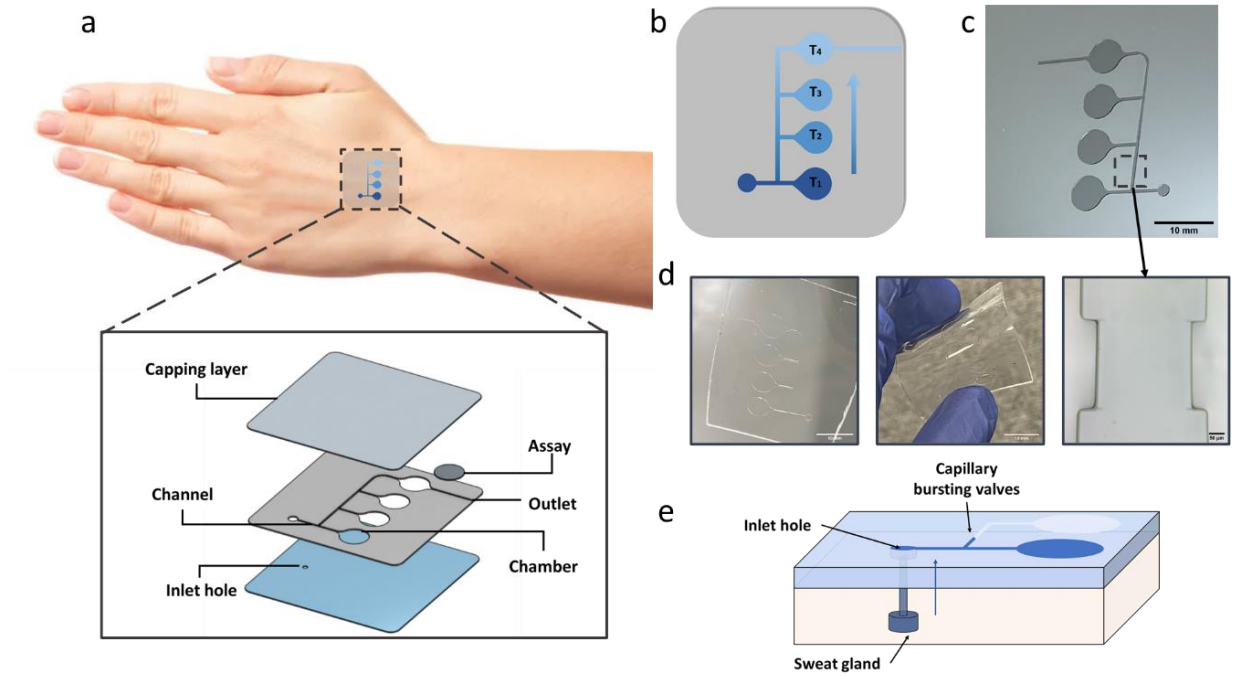


**Figure 2.** Schematic and optical images of an epidermal patch for colorimetric analysis. (a) Exploded view of capping layer, microfluidic layer with channels, an outlet, and an inlet. (b) Schematic of sweat flowing into the chambers sequentially. (c) Optical image of PDMS mould and microscope image of CBVs of PDMS mould. (d) sweat patch in a flat and bent state. (f) Perspective view illustration of sweat patch on skin.

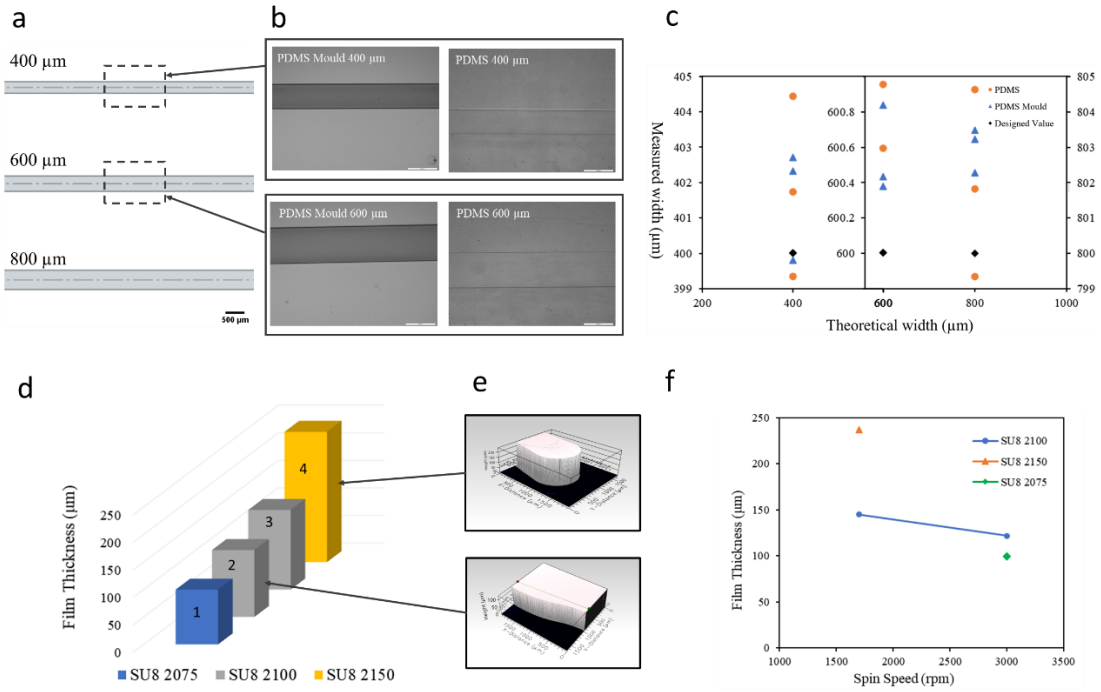


**Figure 3.** Channel width and film thickness analysis. (a) Designed channels with widths of 400 µm, 600 µm and 800 µm. (b) Optical microscope image of channels on PDMS mould and PDMS. (c) Measured width vs. theoretical width (d) Film thickness using three photoresists with different viscosities, (e) Scanned image of sample 4 and sample 2. (f) SU8 2000 film thickness vs. spin speed. Scale bars represent 500 µm in b.

The height of microfluidic channels is determined by viscosity of photoresist and spin speed. (21) Three photoresists with different viscosities and spin speeds (shown as **Table 1**.) were adopted to develop PDMS mould. In **Figure 3. d**, spin speed of sample 1 is the same as that of sample 2 while spin speed of sample 3 is the same as that of sample 4. As the viscosity of photoresist increases, the thickness increases at the same spin speed. When using the same photoresist, the thickness increases with reduced spin speed shown as **Figure 3. f**.

The spin speed affects not only the centrifugal force acting on the photoresist, but also the turbulence of air on the surface of photoresist and the relative velocity of the photoresist and air. The film thickness is the result of a balance between shear stress in the direction tangential to the edge of wafer and the drying (solvent evaporation) rate of photoresist related to viscosity. As the solvent in the photoresist continues to volatilize, the viscosity increases until photoresist can no longer spread in the radial direction driven by centrifugal force. Then, the film thickness does not decrease with extended time. (22)

Besides, temperature and humidity will also affect the fabrication of PDMS mould. (23) The adhesion ability of photoresist decreases in a high relative humidity environment and expansion is more severe in following baking process leading to a thicker film. (24) However, static charges produce and build-up in lower relative humidity environment. There are two baking process in photolithography. (25) The purpose of pre-baking is to evaporate the solvent to enhance the adhesion between photoresist and wafer. The post-baking process is for cross-linking of photoresist after exposure. (26) Short baking time might result in partial polymerization of photoresist and therefore poor pattern developed.

**Table 1.** SU8 viscosity, experimental conditions, and average thickness of PDMS mould

| Photoresist | Viscosity (27) (cSt) | Temperature (°C) | Humidity | Average Thickness (µm) |
|---|---|---|---|---|
| SU8 2075 | 22000 | 22.5 | 46% | 99.56 |
| SU8 2100 | 45000 | 21.8 | 45% | 121.63 |
| SU8 2100 | 45000 | 22.8 | 37% | 144.68 |
| SU8 2150 | 80000 | 22.6 | 54% | 236.98 |

## Capillary bursting valves in microchannels

Three CBVs are design to drive sweat into reservoirs sequentially by blocking sweat flow until the previous reservoir is full as **Figure 4. a**. The following explores the bursting pressure generated by single CBV.

The bursting pressure of rectangular channels is demonstrated by Young-Laplace equation,

$$BP = -2\sigma[\frac{cos(\theta_A + \beta)_{min}}{d} - \frac{\cos\theta_A}{h}]$$

where $\sigma$ is surface tension of liquid, $\theta_A$ is contact angle of channel, $\beta$ is diverging angle, $d$ is width and $h$ is height of the diverging channel as **Figure 4, b**. (7,28)

Here, $\beta$ is 90° and $\theta_A$ is approximately 120° (stationary contact angel of water on PDMS). (7)

The equation can be written as,

$$BP = -2\sigma[\frac{\cos 180°}{d} + \frac{\cos 120°}{h}]$$

The surface tension $\sigma$ here can be regarded as a constant due to slight change of temperature and component of sweat and $h$ is depended on the thickness of microfluidic channels. Thus, $BP$ can be demonstrated as a function which is positively correlated with width of diverging channel.

The predicted bursting pressure for CBVs with different widths are shown as **Figure 4. d**.

Follow-up experiments are required to verify the consistency of calculated values and actual values and determine the optimal width of CBVs.

## Surface modification of microfluidic channels

At present, liquid is driven into channels by external pumps for most of the microfluidic devices in vitro. (29) However, it is inconvenient to introduce such a pump on wearable device. Normally, the sweat does not flow spontaneously in PDMS microfluidic channels due to its hydrophobic nature. After channels surface is modified into hydrophilic or even super-hydrophilic, the sweat can be driven to flow in channels due to negative capillary bursting pressure. (30) Air or oxygen plasma treatment is a common way to change surface hydrophilicity. The air or oxygen plasma modifies the surface by reacting with highly reactive oxygen radicals to introduce active groups such as hydroxyl group $(-OH)$ on the surface. (31) The monomer $O - Si(CH_3)_2$ on PDMS surface is modified into $Si - OH$ as **Figure 4. f**. (32) Due to introduction of functional groups, the hydrophilicity of the

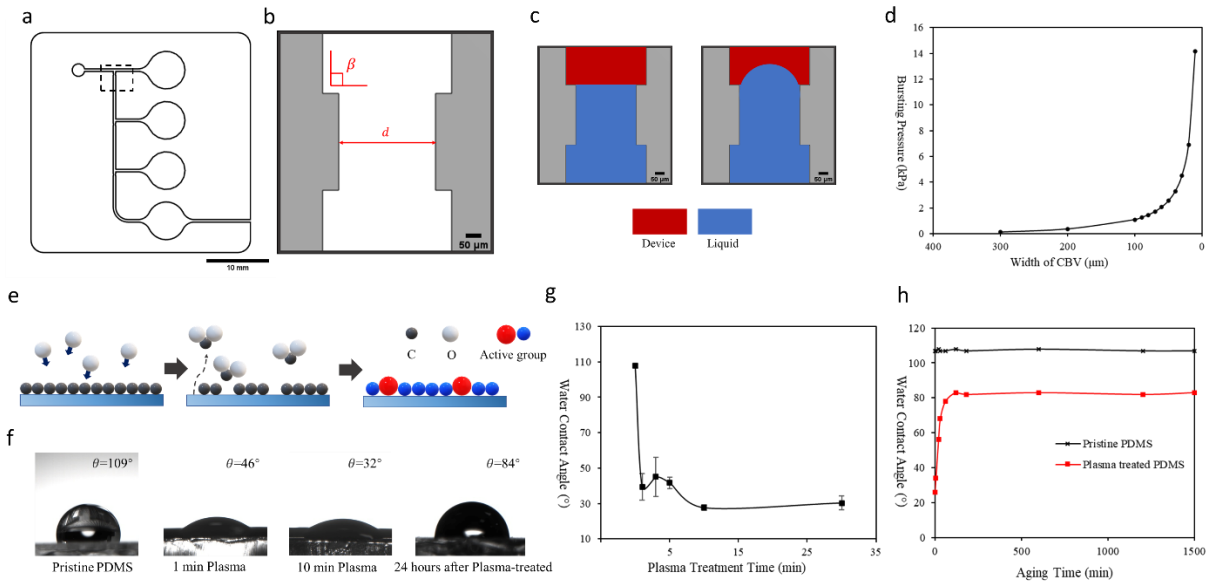


**Figure 4.** (a) Top view illustration of microfluidic layer with CBVs. (b) Schematic diagram of CBV. (c) Schematic of liquid flowing past a CBV. (d) Calculated bursting pressure of CBVs with different widths. (e) Schematic of the mechanism of plasma treatment. (f) Contact angles of pristine PDMS, PDMS with 1 min, 10min plasma treatment and PDMS placed 24 hours after treatment. (g) Contact angles of PDMS with different treatment time. (h) Contact angles of pristine and treated PDMS placed at ambient temperature for different time.

surface will be enhanced.

To investigate the effect of plasma treatment time on hydrophilicity, PDMS samples are subjected to air plasma with 1min, 2min, 5min, 10min and 30min, respectively. The contact angles of PDMS greatly decreased after plasma treatment for 1min. The contact angle tends to be stable even for a longer treatment (**Figure 4. g.**). However, surface hydrophilicity caused by plasma treatment do not last a long time. A quick hydrophobic recover happened at ambient temperature as **Figure 4. h.** due to polymer chain rearrangement to reduce surface energy. (18) To obtain a persisting hydrophilicity, further modifications are needed. Thiol-ene click reaction is a powerful intermediate reaction to introduce any functional groups. It has been experimentally proved that thiols with hydrophilic as $-R$ in following formula have a significant and lasting improvement in surface hydrophilicity. (33)

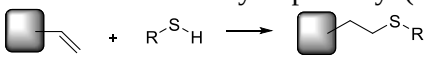


Cysteamine hydrochloride ($C_2H_8ClNS$) which includes an amine( $-NH_2$) can have significant modification of surface hydrophilicity. (**Figure 5.**)

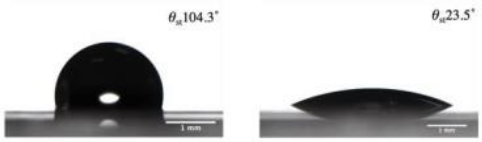


Figure 5. Contact angles before and after cysteamine hydrochloride modified

**Wearable device for electronic sensing**

The wearable device for electronic sensing is composed of three parts shown as **Figure 5. (a)**: (1) a 3D-printed sensor carrier, (2) a microfluidic sweat patch and (3) a bandage to fix the device on wrist.

The 3D-printed sensor carrier was made by a transparent, rigid plastic and designed to hold a PCB board firmly as **Figure 5. (c**). The sensor contacts sweat in chamber and carry out data collection. A silicone gasket is introduced between sensor and chamber to avoid the leakage of sweat as **Figure 5. (d**). When the chamber is full filled with sweat, the channel will lead the sweat to the outlet and allow it to drain from the device.

The microfluidic sweat patch was made by PDMS, a transparent and biocompatible material as mentioned before. In **Figure 5. (e)**, The channels on sweat patch are designed to be petal-shaped which increasing the contact area with sweat glands to collection sweat as much as possible. The microfluidic layer includes a collection of microchannels (gradient increase from ~400 μm to ~1mm in width) and a chamber (~3 mm in radius) and an inlet (~1.5 mm in diameter). The small thickness (~ 0.5 mm) and flexibility of this patch allow it to be mounted better on skin.

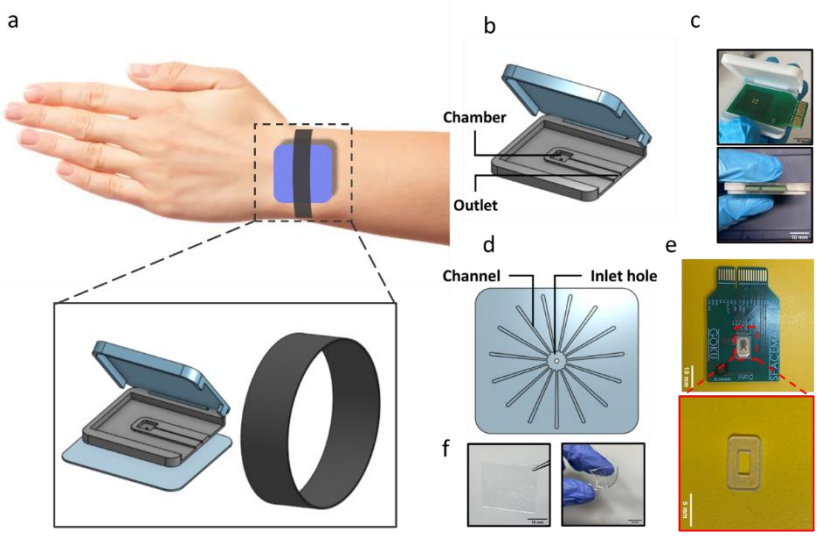


**Figure 5.** Schematic and optical images of a wearable device for electronic sensing. (a) Overview of the components of the wearable device. (b) A 3D-printed plastic sensor carrier with an inlet, an outlet and a camber. (c) Optical image of sensor carrier with PCB board. (d) Optical image silicone gasket to avoid the leakage of sweat, (e) A PDMS microfluidic sweat patch with petal-shaped channels, (f) Optical image of sweat patch in a flat and bent state.

## Conclusion

In results, two wearable microfluidic device prototypes for sweat sensing are designed and fabricated. Channels with hundreds of microns can be developed precisely by photolithography process. In fabrication of channels, the thickness control is difficult due to influence of multiple factors including photoresist viscosity, spin speed, relative humidity, and baking conditions. Viscosity of photoresist is the most important factor among them which determines upper and lower limits. Therefore, after designing a channel with a certain thickness, it is necessary to determine photoresist first, and then adjust other parameters according to actual results. The capillary bursting valve offer a bursting pressure for sweat to pass which can help achieve staged sweat sensing. Surface modification by plasma treatment enhanced wetting of channels to some extends. To maintain that nature, subsequent modification is needed for spontaneous sweat collection. Besides, the applications of the devices also need to be developed such as introducing enzyme assays or electronic sensors in chambers to study the feasibility for sweat sensing of the devices.

## Acknowledgements

## References


1. Ribnicky DM, Komarnytsky S, Poulev A, Borisjuk N, Brinker A, Moreno DA, et al. *PII: S0167-7799(02)02080-2*. TRENDS in Biotechnology. 2002. http://tibtech.trends.com0167-7799/02/$-seefrontmatter
2. McNaney R, Vines J, Roggen D, Balaam M, Zhang P, Poliakov I, et al. Exploring the acceptability of google glass as an everyday assistive device for people with Parkinson's. In: *Conference on Human Factors in Computing Systems - Proceedings*. Association for Computing Machinery; 2014. p. 2551–2554. https://doi.org/10.1145/2556288.2557092.
3. Brabazon T. Digital fitness: Self-monitored fitness and the commodification of movement. *COMMUNICATION POLITICS & CULTURE*. 2015;48(2): 1–23.
4. Apple. *iWatch*. Apple (United Kingdom).
5. Yang Y, Gao W. *Wearable and flexible electronics for continuous molecular monitoring*. Chemical Society Reviews. 2019. p. 1465–1491. https://doi.org/10.1039/c7cs00730b.
6. Sempionatto JR, Martin A, García-Carmona L, Barfidokht A, Kurniawan JF, Moreto JR, et al. Skin-worn Soft Microfluidic Potentiometric Detection System. *Electroanalysis*. 2019;31(2): 239–245. https://doi.org/10.1002/elan.201800414.
7. Choi J, Xue Y, Xia W, Ray TR, Reeder JT, Bandodkar AJ, et al. Soft, skin-mounted microfluidic systems for measuring secretory fluidic pressures generated at the surface of the skin by eccrine sweat glands. *Lab on a Chip*. 2017;17(15): 2572–2580. https://doi.org/10.1039/c7lc00525c.
8. Zhang Y, Guo H, Kim SB, Wu Y, Ostojich D, Park SH, et al. Passive sweat collection and colorimetric analysis of biomarkers relevant to kidney disorders using a soft microfluidic system. *Lab on a Chip*. 2019;19(9): 1545–1555. https://doi.org/10.1039/c9lc00103d.
9. Stroock AD. Chapter 17 - MICROFLUIDICS. In: Ligler FS, Taitt CR (eds.) *Optical Biosensors (Second Edition)*. Second Edition. Amsterdam: Elsevier; 2008. p. 659–681. https://doi.org/https://doi.org/10.1016/B978-044453125-4.50019-X.
10. Kim J, Campbell AS, de Ávila BEF, Wang J. Wearable biosensors for healthcare monitoring. *Nature Biotechnology*. 2019;37(4): 389–406. https://doi.org/10.1038/s41587-019-0045-y.
11. Mere L, Bennett T, Coassin P, England P, Hamman B, Rink T, et al. Miniaturized FRET assays and microfluidics: key components for ultra-high-throughput screening. *Drug Discovery Today*. 1999;4(8): 363–369. https://doi.org/https://doi.org/10.1016/S1359-6446(99)01377-X.
12. Quero RF, de Castro Costa BM, da Silva JAF, de Jesus DP. Using multi-material fused deposition modeling (FDM) for one-step 3D printing of microfluidic capillary electrophoresis with integrated electrodes for capacitively coupled contactless conductivity detection. *Sensors and Actuators B: Chemical*. 2022;365: 131959. https://doi.org/https://doi.org/10.1016/j.snb.2022.131959.
13. Huang Y, Liu S, Yang W, Yu C. Surface roughness analysis and improvement of PMMA-based microfluidic chip chambers by CO2 laser cutting. *Applied Surface Science*. 2010;256(6): 1675–1678. https://doi.org/https://doi.org/10.1016/j.apsusc.2009.09.092.
14. Michael Dwamena. *Is 100 Microns Good for 3D Printing? 3D Printing Resolution*. 3D Printerly.
15. Zhou R, Allsopp DWE, Law ME, Wood J, el Gomati MM. Photoresist silylation and dry development for sub-micron photolithography. *Vacuum*. 1992;43(1): 83–86. https://doi.org/https://doi.org/10.1016/0042-207X(92)90190-8.
16. Niculescu AG, Chircov C, Bîrcă AC, Grumezescu AM. *Fabrication and applications of microfluidic devices: A review*. International Journal of Molecular Sciences. 2021. p. 1–26. https://doi.org/10.3390/ijms22042011.
17. Garcia-Cordero E, Wildhaber F, Bellando F, Longo J, Fernandez-Bolanos M, Guerin H, et al. Embedded passive nano-liter micropump for sweat collection and analysis. In: *Proceedings of the IEEE International Conference on Micro Electro Mechanical Systems (MEMS)*. Institute of Electrical and Electronics Engineers Inc.; 2018. p. 1217–1220. https://doi.org/10.1109/MEMSYS.2018.8346782.
18. Zhou J, Khodakov DA, Ellis A v, Voelcker NH. Surface modification for PDMS-based microfluidic devices. *ELECTROPHORESIS*. 2012;33(1, SI): 89–104. https://doi.org/10.1002/elps.201100482.
19. Reeder JT, Xue Y, Franklin D, Deng Y, Choi J, Prado O, et al. Resettable skin interfaced microfluidic sweat collection devices with chemesthetic hydration

feedback. *Nature Communications*. 2019;10(1). https://doi.org/10.1038/s41467-019-13431-8.
20. Kalin M, Polajnar M. The Effect of Wetting and Surface Energy on the Friction and Slip in Oil-Lubricated Contacts. *Tribology Letters*. 2013;52(2): 185–194. https://doi.org/10.1007/s11249-013-0194-y.
21. Huang Z, Li X, Martins-Green M, Liu Y. Microfabrication of cylindrical microfluidic channel networks for microvascular research. *Biomedical Microdevices*. 2012;14(5): 873–883. https://doi.org/10.1007/s10544-012-9667-2.
22. Tyona MD. A theoritical study on spin coating technique. *Advances in materials Research*. 2013;2(4): 195–208. https://doi.org/10.12989/amr.2013.2.4.195.
23. Chang-Yen DA, Eich RK, Gale BK. A Monolithic PDMS Waveguide System Fabricated Using Soft-Lithography Techniques. *J. Lightwave Technol.* 2005;23(6): 2088. http://opg.optica.org/jlt/abstract.cfm?URI=jlt-23-6-2088
24. Hu DC, Chen HC. Humidity effect on polyimide film adhesion. *Journal of Materials Science*. 1992;27(19): 5262–5268. https://doi.org/10.1007/BF00553402.
25. Cruise RD, Hadler K, Starr SO, Cilliers JJ. The effect of particle size and relative humidity on triboelectric charge saturation. *Journal of Physics D: Applied Physics*. 2022;55(18). https://doi.org/10.1088/1361-6463/ac5081.
26. Lau KH, Giridhar A, Harikrishnan S, Satyanarayana N, Sinha SK. Releasing high aspect ratio SU-8 microstructures using AZ photoresist as a sacrificial layer on metallized Si substrates. *Microsystem Technologies*. 2013;19(11): 1863–1871. https://doi.org/10.1007/s00542-013-1740-0.
27. MicroChem. *SU-8 2000 Data Sheet (2100-2150)* . MicroChem.
28. Huang CP, Lu J, Seon H, Lee AP, Flanagan LA, Kim HY, et al. Engineering microscale cellular niches for three-dimensional multicellular co-cultures. *Lab on a Chip*. 2009;9(12): 1740–1748. https://doi.org/10.1039/b818401a.
29. Komeya M, Hayashi K, Nakamura H, Yamanaka H, Sanjo H, Kojima K, et al. Pumpless microfluidic system driven by hydrostatic pressure induces and maintains mouse spermatogenesis in vitro. *Scientific Reports*. 2017;7(1). https://doi.org/10.1038/s41598-017-15799-3.
30. Wang S, Zhang X, Ma C, Yan S, Inglis D, Feng S. A Review of Capillary Pressure Control Valves in Microfluidics. *Biosensors*. 2021;11(10). https://doi.org/10.3390/bios11100405.
31. Siow KS, Britcher L, Kumar S, Griesser HJ. Plasma Methods for the Generation of Chemically Reactive Surfaces for Biomolecule Immobilization and Cell Colonization - A Review. *Plasma Processes and Polymers*. 2006;3(6–7): 392–418. https://doi.org/https://doi.org/10.1002/ppap.200600021.
32. Jiang B, Guo H, Chen D, Zhou M. Microscale investigation on the wettability and bonding mechanism of oxygen plasma-treated PDMS microfluidic chip. *Applied Surface Science*. 2022;574. https://doi.org/10.1016/j.apsusc.2021.151704.
33. Ueda E, Feng W, Levkin PA. Superhydrophilic–Superhydrophobic Patterned Surfaces as High-Density Cell Microarrays: Optimization of Reverse Transfection. *Advanced Healthcare Materials*. 2016;5(20): 2646–2654. https://doi.org/https://doi.org/10.1002/adhm.201600518.